Title

Effect of scanning beam size on the lateral resolution of mouse retinal imaging with SLO.

Journal

Optics Letters, 40(24)

ISSN

0146-9592

Authors

Zhang, Pengfei
Goswami, Mayank
Zam, Azhar
et al.

Publication Date

2015-12-15

DOI

10.1364/ol.40.005830

Peer reviewed

HHS Public Access

Author manuscript

Opt Lett. Author manuscript; available in PMC 2016 June 21.

Published in final edited form as:

Opt Lett. 2015 December 15; 40(24): 5830–5833.

Effect of scanning beam size on the lateral resolution of mouse retinal imaging with SLO

Pengfei Zhang[1], **Mayank Goswami**[1], **Azhar Zam**[1], **Edward N. Pugh**[1], and **Robert J. Zawadzki**[1,2,*]

[1]UC Davis RISE Eye-Pod Small Animal Imaging Laboratory, Department of Cell Biology and Human Anatomy, University of California Davis, 4320 Tupper Hall, Davis, California 95616, USA

[2]UC Davis Eye Center, Department of Ophthalmology & Vision Science, University of California Davis, 4860 Y Street, Suite 2400, Sacramento, California 95817, USA

Abstract

Scanning laser ophthalmoscopy (SLO) employs the eye's optics as a microscope objective for retinal imaging *in vivo*. The mouse retina has become an increasingly important object for investigation of ocular disease and physiology with optogenetic probes. SLO imaging of the mouse eye, in principle, can achieve submicron lateral resolution thanks to a numerical aperture (NA) of ~0.5, about 2.5 times larger than that of the human eye. In the absence of adaptive optics, however, natural ocular aberrations limit the available optical resolution. The use of a contact lens, in principle, can correct many aberrations, permitting the use of a wider scanning beam and, thus, achieving greater resolution then would otherwise be possible. In this Letter, using an SLO equipped with a rigid contact lens, we report the effect of scanning beam size on the lateral resolution of mouse retinal imaging. Theory predicts that the maximum beam size full width at half-maximum (FWHM) that can be used without any deteriorating effects of aberrations is ~0.6 mm. However, increasing the beam size up to the diameter of the dilated pupil is predicted to improve lateral resolution, though not to the diffraction limit. To test these predictions, the dendrites of a retinal ganglion cell expressing YFP were imaged, and transverse scans were analyzed to quantify the SLO system resolution. The results confirmed that lateral resolution increases with the beam size as predicted. With a 1.3 mm scanning beam and no high-order aberration correction, the lateral resolution is ~1.15 μm, superior to that achievable by most human AO-SLO systems. Advantages of this approach include stabilization of the mouse eye and simplified optical design.

Scanning laser ophthalmoscopy (SLO) is a non-invasive retinal imaging modality that is widely used as diagnostic tool in clinical ophthalmology and basic vision science research, including longitudinal studies in living animals [1›2]. A great advantage of SLO is its ability to generate images, not only from light reflected from the retina, but also from fluorescence. In addition, the confocal nature of SLO helps it reject out-of-focus light, improving image

*Corresponding author: rjzawadzki@ucdavis.edu.

OCIS codes: (170.4460) Ophthalmic optics and devices; (170.5755) Retina scanning; (170.4470) Ophthalmology; (170.2520) Fluorescence microscopy; (170.1790) Confocal microscopy; (170.5810) Scanning microscopy.

contrast. Applied to mice, SLO also affords the possibility of imaging single cells and their functional properties labeled by cell-specific fluorescent proteins introduced into the retina, either through genetic engineering or by viral-mediated gene transfer [3–6].

The maximum available numerical aperture (NA) of the mouse eye is more than twice that of the human eye [7], so the mouse's eye potentially offers a substantially higher optical resolution. However, similar to the situation in human eyes, ocular aberrations are expected to preclude use of the full mouse pupil for SLO without implementation of adaptive optics. Nonetheless, depending on the profile and magnitude of the aberrations of the mouse eye, it can be anticipated that increasing the scanning beam width (thereby increasing the NA of the incoming light) in an SLO should improve image resolution, as it does in confocal laser scanning microscopy (CLSM). However, predicting the consequences of varied beam size is complicated both by the specific profile of ocular aberrations and by the fact that the SLO, like the CLSM, is a two-pass optical system, so that light outgoing through the dilated mouse pupil is also subject to aberrations that may not affect the incoming beam. Therefore, we undertook a study of the relationship between the scanning beam size at the mouse eye pupil and SLO lateral resolution for *in vivo* mouse retina imaging to find the beam size that offers the best performance. In this investigation, we used a custom mouse SLO system, employing a rigid mouse contact lens [8] to image retinal ganglion cells that express yellow fluorescent protein (YMP) in a *B6.Thy1-YFP-H* mouse, and quantified the system's resolution by measuring the FWHM of the cell dendrites' line spread function, as was recently used by Geng *et al*. [9].

The experimental results presented in this Letter were acquired with a multimodal OCT/SLO mouse retinal imaging system [8]. Here we will only describe the SLO subsystem. Only two of three SLO detection channels were used in the experiments presented here: one for back-reflected light (PMT1) and one for fluorescence (PMT2). A supercontinuum laser (Fianium, SC-400) served as the light source; when filtered by a bandpass filter 1 (centered at 490 nm; 6.8 nm bandwidth), the laser provided 80 μW illumination at the mouse pupil. The scanning duration for any specific imaging location did not exceed 5 min, and the time-integrated scanning energy densities (J/deg^2) were lower than those reported by Geng *et al*. [9]. A long-pass filter (filter 2, Semrock FF01-503/LP) was used for collection of YFP emission. PMT1 and PMT2 (Hamamatsu, H7422-20, H7422-40) detected the back-reflected and YFP fluorescence light, respectively.

The *B6.Thy1-YFP-H* mouse was obtained from Jackson Labs. Its husbandry and handling were in accord with protocols approved by the University of California Animal Care and Use Committee (IACUC), which strictly adhere to all NIH guidelines. During image acquisition, the mouse was anesthetized with the inhalational anesthetic isoflurane (2-3% in O_2). The pupil was dilated with tropicamide (1%) and phenylephrine (2.5%), and the cornea was kept hydrated by means of a gel (Gel Tears, Chem-Pharm Fabrik, Berlin, DE) covered by a contact lens [0 Diopters (Dpt.)] with 1.65 mm radius of curvature, Unicon Corporation (marked by a red arrow in Fig. 1).

The laser input was introduced by a single-mode fiber (460 HP, Thorlabs, 3.5 μm core size with 0.13 NA) and collimated with an 11 mm focal length aspheric lens (L_{ls}, C220TME-A,

Thorlabs). Changes in the beam size at the mouse pupil, in principle, could be achieved by varying the beam size at the light input. However, in our system the size of the galvanometer mirrors (Cambridge Technology, 6215H) limits the imaging beam size. Thus, we used a different approach to resize the beam at the mouse pupil, changing the magnification of the imaging telescope L1 and tube lens L2 pairs, Fig. 1.

The FWHM of the imaging beam on the scanning mirror was measured with a CMOS camera (5.3 μm pixel size, Thorlabs, DCC1240M-GL) and found to be 1.70±0.07 mm. In both detection channels, the light was collected by an objective lens (L-4X, Newport) with 45.5 mm focal length into a multimode fiber with 50 μm core size: thus, the ratio of the pinhole diameter to Airy disk ranged from 2 to 3 for the three beam sizes in this study. The XY scanner mirrors determined the exit aperture size for the 0.46 and 0.84 mm beams, while the dilated pupil dictated the limiting exit aperture diameter for the 1.32 mm beam. Taking these factors into consideration—the incoming laser beam diameter, the pinhole size, and the NAs of the input and output—the system's PSF can be calculated as follows [10¯12]:

$$PSF = (P_{\text{in}} \otimes (M_{\text{ls}} \cdot S_{\text{ls}})) \cdot (P_{\text{out}} \otimes (M_{\text{det}} \cdot S_{\text{det}})). \quad (1)$$

Here, P_{in} and P_{out} are the PSFs determined by the input and output NAs acting alone, respectively; S_{ls} and S_{det} are the size of the fiber cores in the light source and the detection channel, which must be scaled by magnification factors M_{ls} and M_{det} to their size in the image plane (mouse retina). The magnification factors can be calculated as [11]

$$M_{\text{ls}} = \frac{f_{\text{L1}}}{f_{\text{ls}}} \cdot \frac{f_{\text{mouse}}}{f_{\text{L2}}}; M_{\text{det}} = \frac{f_{\text{L1}}}{f_{\text{det}}} \cdot \frac{f_{\text{mouse}}}{f_{\text{L2}}} = \frac{f_{\text{ls}}}{f_{\text{det}}} \cdot M_{\text{ls}}, \quad (2)$$

where f_{ls} is the focal length (11 mm) of the collimator (L_{ls}) for the light source; f_{det} is the focal length (45.5 mm) of the detection lens (L_{det}); f_{L1}, f_{L2}, are the focal lengths of lenses L1, L2, respectively; f_{mouse} (1.95 mm) is the focal length of the mouse eye.

To evaluate the effect of the ocular aberrations of the mouse eye on the lateral PSF, we simulated two aberrated wavefronts at the pupil plane using measured mouse ocular aberrations expressed in terms of Zernike polynomials, as reported in [7]. The values of the Zernike polynomial coefficients used are shown in the left part of Fig. 2(a). Because the reported coefficients are averages from 10 mouse eyes, they underestimate the aberrations in a typical mouse eye without a contact lens. Thus, in the simulations, we decided to increase each coefficient by the reported standard error of the mean (SEM) to make these aberrations more representative of those of an individual mouse eye with a contact lens: the representative modeled wavefronts arising from SEM-augmented Zernike coefficients are shown in the right-hand portion of Fig. 2(a). The defocus term was set to zero because it can be eliminated by moving the contact lens axially to change the thickness of the gel between the cornea and the contact lens. After calculating the PSF of the simulated system for different scanning beam sizes, we measured the average diameter $\overline{FWHM}_D$ at the 50% radial profiles of the PSF, calculated by $\overline{FWHM}_D = 2 \cdot \sqrt{A/\pi}$, where A is the area

enclosing PSF intensities above half-maximum. (This reduces to the conventional definition when the PSF is radially symmetric.) The simulated SLO resolutions for different scanning beam sizes are shown in Fig. 2(b). The FWHMs of the “left eye” and “right eye” pupils were averaged to keep the figure concise. The simulations show that it is possible to achieve a resolution close to the diffraction limit for pupil sizes smaller than 0.6 mm for the “mean” aberration model. Although the PSF becomes more irregular when the scanning beam size is larger than 0.6 mm, the resolution nonetheless is predicted to increase for beam sizes up to 2 mm. However, little improvement is predicted for scanning beam sizes larger than 1.3 mm.

To examine the effect of scanning beam diameter in the mouse SLO, we employed three pairs of scan lens/tube lens configurations: (1) a 50.8 mm and two 20 mm focal length lenses; (2) a 50.8 mm and a 25 mm lens; and (3) a 25 mm and a 20 mm lens, respectively. For each pair of lenses, the FWHM of the scanning beam at the mouse pupil was measured by the CMOS camera and found to be 0.46, 0.84, and 1.32 mm, respectively. As a consequence of changing the magnification of this telescope, we also altered the maximum available field of view (FOV) of our imaging system from 51° for the 0.46 mm beam, to 26° for the 0.84 mm beam, and 32° for the 1.32 mm beam. Since, in our system, the FOV depends on the NA of lens L2 (Fig. 1), the 51° FOV, in principle, could be maintained even for the larger beam sizes at the mouse pupil by keeping the same telescope and using larger scanning mirrors.

The example results of imaging retina with these three beam sizes are shown in Fig. 3. First, the 0.46 mm beam was used to get widefield SLO back-reflection and fluorescence images [Figs. 3(a) and 3(b), respectively]. The scanning range was 1700 μm (assuming 34 μm/deg) for the full FOV. A zoomed-in scan [Fig. 3(c)] was performed in the region with single ganglion cell with strong YFP fluorescence, so that the image resolution is limited by the optics, not by the sampling. The zoomed-in scan ROI was 9 × 9 deg or 306 μm × 306 μm. The cell’s axon and the dendrites are clearly resolved in the zoomed-in view.

We then switched to the 0.84 mm scanning beam diameter and imaged the same cell. The image was aligned to that of Fig. 3(c) with the Fiji ImageJ “affine” function to get Fig. 3(d). An additional zoomed-in scan was taken of the upper left portion of the cell [Fig. 3(e), 116 μm × 116 μm] to further increase spatial sampling and ensure that the image was limited only by the optical resolution.

Finally, the 1.32 mm scanning beam was used to image the lower right portion of the cell [Fig. 3(f), 116 μm × 116 μm]. By comparison, with published *ex vivo* confocal and *in vivo* AO-SLO images of a single ganglion cell from a mouse of the same genotype [9], it is clear that the discontinuities of YFP fluorescence in the dendrites in this figure give actual dendritic structural information, revealing a higher resolution than the images in Fig. 3 obtained with smaller size beams.

To quantify the lateral resolution, three ganglion cell dendrites that were in sharp focus in each image were selected [green and red arrows in Figs. 3(c)–3(f)]; only the line profiles from the green arrows were plotted in Fig. 4(a). Gaussian functions were then fitted to the intensity profiles taken along lines perpendicular to the dendrites. Four of the intensity

profiles (green arrow pointed in each image) and their Gaussian profiles are plotted in Fig. 4(a). The data show that the resolution was improved with increased scanning beam size at the mouse pupil, as further illustrated in Fig. 4(b). The average FWHMs are 2.90 ± 0.13, 1.86 ± 0.03, 1.60 ± 0.09, and 1.26 ± 0.03 μm for the 0.47, 0.84, 0.84 (zoomed-in scan), and 1.32 (zoomed-in scan) mm size beams, respectively. These FWHMs represent the system's PSF convolved with the ganglion cell dendrites (typically, 0.7 μm). To compare these results with our theoretical model, we calculated the FWHMs of the diffraction-limited PSF and mouse ocular aberration model's PSF after convolving with a 0.7 μm wide line object. To consider asymmetry in the model's PSF, the convolution was conducted with the line object at both vertical and horizontal orientations, and the average FWHM was recorded, as shown in Fig. 4(b) (blue line and blue dots). Taking into account dendrite diameter, we estimate the system resolution for the 1.32 mm scanning beam size to be around 1.15 μm.

The scanning beam size influences both axial and lateral resolution. Given that lateral resolution depends on the inverse of the NA and axial resolution depends on the inverse of NA^2, separate studies should be performed to evaluate the effect of pupil size on axial resolution [13]. Thus, using the pupil size that optimizes lateral resolution will also improve axial sectioning relative to that of the system using a smaller scanning beam size (smaller NA). Figures 5(a) and 5(b) show the back-reflection images simultaneously acquired with Figs. 3(c) and 3(f): these images clearly reveal the effect of increased axial resolution (confocal sectioning) by resolving the nerve fiber bundles and capillaries (red and green arrows pointed) in Fig. 5(b), which are not clearly visible in Fig. 5(a). On the other hand, the increased axial sectioning capability makes it more difficult to bring the objects into focus in our current setup. A focusing capability will need to be included with an SLO system if the high-resolution capability of the large scanning beam size is to be fully utilized.

We noticed that in our experiments there is no obvious reduction in image quality, even for the 1.32 mm beam size. This is probably due to the fact that the ocular aberrations reported in [7] were measured in mice eyes without a contact lens while, in our system, a 0 Dpt. rigid contact lens was always used to keep the cornea hydrated. In this system, the contact lens constitutes the primary refractive element of the eye, so that most refractive errors arising from the corneal front surface are canceled.

In summary, as predicted, the scanning beam diameter at the mouse pupil is a major determinant of SLO lateral resolution. In our custom SLO, the beam size was varied, allowing characterization of the system resolution. Our study shows that, by using a relatively large scanning beam size, mouse retinal SLO can achieve a FWHM lateral resolution of 1.15 μm without additional aberration corrections. Interestingly, this lateral resolution is greater than that of most human AO-SLO systems. However, since our imaging system does not implement AO, its performance will depend on the ocular aberrations of the individual mouse. The modeling of ocular aberrations in this Letter was based on reported averaged values of Zernike coefficients and their SEM from mouse eyes without a contact lens, and likely underestimates the aberrations of any individual mouse. This model is nonetheless useful for predicting deviations from the diffraction-limited performance of an SLO system with a contact lens. In the future, studies of the field dependence of aberrations (as recently presented for humans [14,15]) of individual mice of different strains and ages

with and without a contact lens will be needed. Such studies will be necessary to evaluate the full benefits of using a contact lens for imaging with beams of various sizes and at different retinal eccentricities, and help to inform the design of future mouse retinal imaging systems. Nevertheless, our results suggest that application of AO for mouse retinal imaging might be needed only if higher lateral resolution or precise axial sectioning than reported in this Letter is desired, or for efficient nonlinear (e.g., two-photon [16]) optical imaging. Based on these results, we also conclude that high lateral resolution mouse retinal SLO systems require an active axial focusing capability. This need arises from the increased axial sectioning that accompanies increased lateral resolution of these systems.

In conclusion, as already demonstrated in literature [5,8], high-resolution mouse SLO without AO may be sufficient for many *in vivo* studies of morphology and function of fluorescently labeled retinal cells, allowing wider fields of view and enhancing the ability to perform longitudinal imaging of the same group of cells.

Acknowledgment

The authors thank Drs. Marie Burns and John S. Werner for their help and support.

Funding. National Institutes of Health (NIH) (EY012576, EY02660, EY14047); National Science Foundation (NSF) (I/UCRC CBSS); University of California, Davis (Research in Science & Engineering [RISE]).

REFERENCES

1. Webb RH, Hughes GW. IEEE Trans. Biomed. Eng. 1981; BME-28:488. [PubMed: 7275128]
2. Sharp PF, Manivannan A, Xu H, Forrester JV. Phys. Med. Biol. 2004; 49:1085. [PubMed: 15128191]
3. Seeliger MW, Beck SC, Pereyra-Munoz N, Dangel S, Tsai JY, Luhmann UFO, van de Pavert SA, Wijnholds J, Samardzija M, Wenzel A, Zrenner E, Narfstrom K, Fahl E, Tanimoto N, Acar N, Tonagel F. Vis. Res. 2005; 45:3512. [PubMed: 16188288]
4. Paques M, Sirnonutti M, Roux MJ, Picaud S, Levavasseur E, Bellman C, Sahel JA. Vis. Res. 2006; 46:1336. [PubMed: 16289196]
5. Alt C, Runnels JM, Teo GSL, Lin CP. IntraVital. 2014; 1:132.
6. Zawadzki RJ, Zhang P, Zam A, Miller EB, Goswami M, Wang X, Jonnal RS, Lee S, Kim DY, Flannery JG, Werner JS, Burns ME, Pugh EN. Biomed. Opt. Express. 2015; 6:2191. [PubMed: 26114038]
7. Geng Y, Schery LA, Sharma R, Dubra A, Ahmad K, Libby RT, Williams DR. Biomed. Opt. Express. 2011; 2:717. [PubMed: 21483598]
8. Zhang P, Zam A, Jian Y, Wang X, Li Y, Lam KS, Burns ME, Sarunic MV, Pugh EN, Zawadzki RJ. J. Biomed. Opt. 2015 accepted.
9. Geng Y, Dubra A, Yin L, Merigan WH, Sharma R, Libby RT, Williams DR. Biomed. Opt. Express. 2012; 3:715. [PubMed: 22574260]
10. Wilson, T.; Sheppard, C. Theory and Practice of Scanning Optical Microscopy. Academic; 1984. p. 12-122.
11. Webb RH. Rep. Prog. Phys. 1996; 59:427.
12. Mueller, M. Introduction to Confocal Fluorescence Microscopy. 2nd ed. SPIE; 2005. p. 1-58.
13. Donnelly WJ, Roorda A. J. Opt. Soc. Am. A. 2003; 20:2010.
14. Nowakowski M, Sheehan M, Neal D, Goncharov AV. Biomed. Opt. Express. 2012; 3:240. [PubMed: 22312578]
15. Polans J, Jaeken B, McNabb RP, Artal P, Izatt JA. Optica. 2015; 2:124.

16. Stremplewski P, Komar K, Palczewski K, Wojtkowski M, Palczewska G. Biomed. Opt. Express. 2015; 6:3352. [PubMed: 26417507]

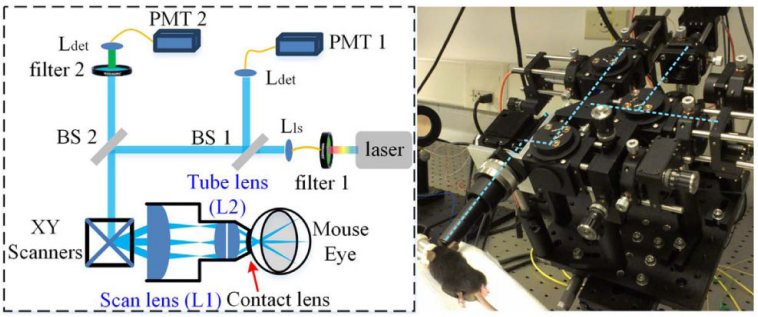

Fig. 1.

Scanning laser ophthalmoscopy (SLO) subsystem schematic (inset at lower right: photo of mouse positioned for imaging with combined OCT/SLO. Dashed blue lines represent paths of imaging beam after exiting the eye). BS 1, beam splitter (50:50); BS 2, beam splitter [70 (T):30(R)]; PMT, photomultiplier tubes; L, lens.

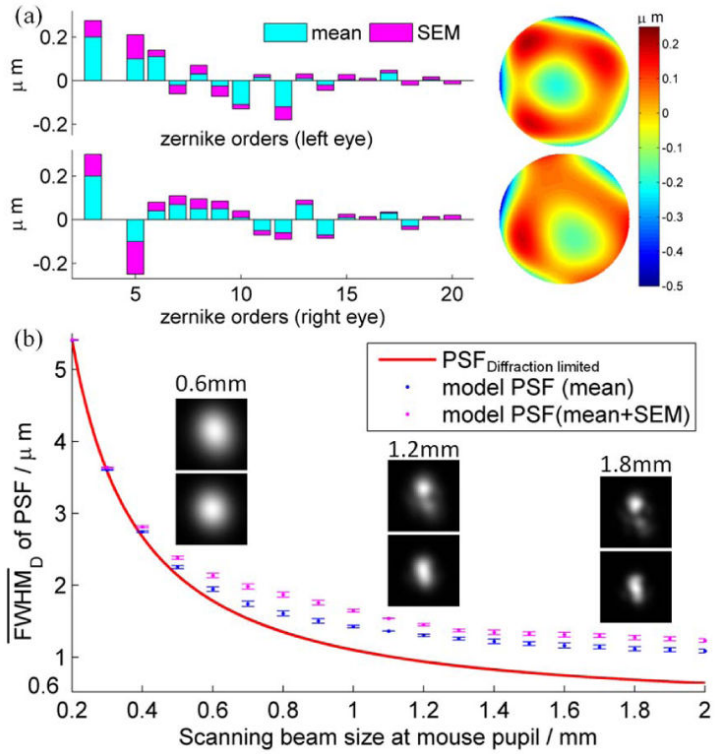

Fig. 2.

Prediction of the lateral resolution at the mouse retina as a function of scanning beam size. (a) Zernike polynomial coefficients taken from [7] for a 2 mm mouse pupil with defocus removed (the coefficients are averages from 10 mice) and the corresponding wavefront predictions (“mean + SEM”). (b) FWHM resolution plotted as a function of the beam size at the pupil (inset shows the PSFs from “left eye”; the top and bottom rows correspond to the “mean + SEM” and “mean” mode, separately). The red line shows the diffraction-limited FWHM (no aberrations).

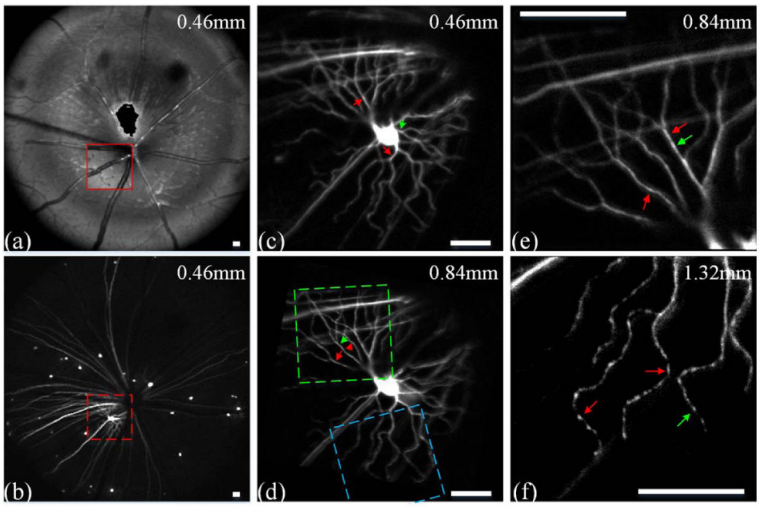

Fig. 3.

SLO images of the retina of a *B6.Thy1-YFP-H* mouse *in vivo*. (a) Widefield back-reflection and (b) fluorescence images with a 0.46 mm scanning beam. A number of fluorescent ganglion cell bodies (bright dots) and axons (bright lines leading to the optic disk) are seen. (c), (d) Zoomed-in scans of the red dashed rectangle area in (b) with 0.46 and 0.84 mm beams, respectively. (e), (f) Zoomed-in scans of the green and blue rectangular areas in (d) with 0.84 mm and 1.32 mm beams, respectively. Scale bar, 50 μm. (The irregular black spot in panel (a) is used to mask a reflection artifact.)

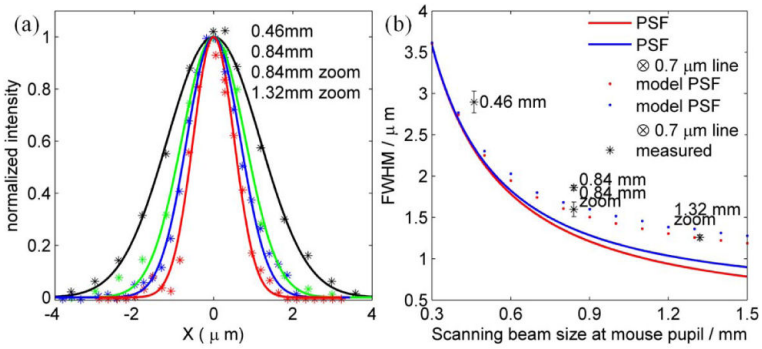

Fig. 4.

Quantification of the imaging system resolution. (a) Line intensity profiles (after DC subtraction and normalization) and their fitted Gaussian profiles of the corresponding dendrites' transverse cross sections (green arrows pointed in Figs. 3(c)–3(f)). (b) Measured FWHM for different scanning beam sizes (black symbols with error bars) plotted along with the predicted PSFs from Fig. 2(b) convolved with a 0.7 um width line object, simulating ganglion cells dendrites.

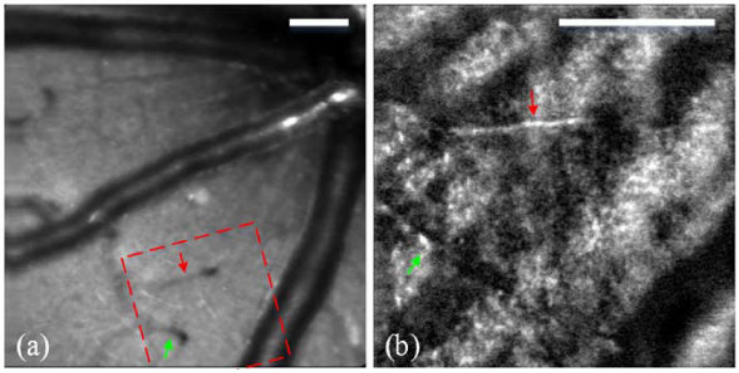

Fig. 5.

In vivo reflectance images of the mouse retina acquired simultaneously with fluorescence images. (a) Reflectance image corresponding to Fig. 3(c). (b) Reflectance image corresponding to Fig. 3(f). [The location of the image in (b) is indicated by the red dashed rectangle in (a)]. Scale bar, 50 μm.